

Investigation of Jahn–Teller splitting with O 1s x-ray absorption spectroscopy in strained Nd_{1-x}Ca_xMnO₃ thin films

Daniel Hsu,¹ Y. S. Chen,^{1,2} M. Y. Song,^{1,3} C. H. Chuang,^{3,4} Minn-Tsong Lin,^{3,5} W. F. Wu,² and J. G. Lin^{1,a)}

¹Center for Condensed Matter Sciences, National Taiwan University, Taipei 106, Taiwan

²Department of Mechanical Engineering, National Taiwan University, Taipei 106, Taiwan

³Department of Physics, National Taiwan University, Taipei 106, Taiwan

⁴National Synchrotron Radiation Research Center, Hsinchu 300, Taiwan

⁵Institute of Atomic and Molecular Sciences, Academia Sinica, Taipei 115, Taiwan

(Received 24 November 2009; accepted 6 January 2010; published online 29 January 2010)

Electronic structures of strained Nd_{1-x}Ca_xMnO₃ (NCMO) thin films with $x=0$ to 0.8 are investigated via x-ray absorption spectroscopy (XAS). The obtained O 1s spectra within the photon energy 529–535 eV can be decomposed into $e_g\uparrow^1$, $e_g\uparrow^2$, $t_{2g}\downarrow$, and $e_g\downarrow$ bands. Based on the assigned energy levels of these band states, the energies of magnetic exchange, crystal field and Jahn–Teller (JT) splitting are determined. Particularly, the JT splitting is around 0.8 eV, which is observed with O 1s XAS for the first time in NCMO thin films. © 2010 American Institute of Physics.

[doi:10.1063/1.3299023]

Perovskite manganites with chemical compositions $Re_{1-x}A_xMnO_3$, where Re is a rare-earth ($Re=La, Pr, \text{ and } Nd$) and A is an alkaline-earth metal ($A=Sr, Ba, \text{ and } Ca$), have activated a great amount of research because of their extraordinary physical properties such as the colossal magnetoresistance (CMR) and the strong correlations of spin, charge, and orbital ordering.^{1–8} In this mixed-valence system of Mn^{3+}/Mn^{4+} , the strong coupling between the magnetic ordering and the electrical conductivity is explained by the double-exchange model, in which the holes in e_g orbitals are the electrical carriers that move on a background of t_{2g} ions.^{3–5} The phase separation exists in these materials and was suggested to be the origin of the CMR effect.^{9–11} One of the important features of these perovskite oxides is the Jahn–Teller (JT) distortion, which is related to the local oxygen octahedra and can be controlled with the effective radius of (R, A)-ion. For example, the O octahedron sustains a stronger static JT distortion in $ReMnO_3$ than $AMnO_3$ due to the high crystal anisotropy.¹² Overall, the electronic properties of $Re_{1-x}A_xMnO_3$ are mainly determined by the state energies of the Mn ($3d$) bands under the combined effects of the crystal field splitting, magnetic exchange and the JT distortion.^{13,14} Based on the theoretical prediction for $LaMnO_3$, the splitting energy should about 3.0 eV due to the magnetic exchange, 2.0 eV from the crystal field, and 1.5 eV from the JT distortion.¹⁵ However, the JT splitting energy was never been confirmed with any experimental evidence.

XAS is a particularly sensitive probe for the electronic structures and thus can provide the direct information about the valence, the unoccupied electronic states, and the effective charge of the absorber atom in a solid.^{16–18} Despite the numerous XAS studies and the related work of electron-energy-loss spectroscopy in CMR materials,^{18–24} there is still lack of information about the splitting energy of JT distortion. Therefore, it is our speculation that the actual JT splitting energy in CMR system may be smaller than the theoret-

ical value, which makes it hard to be detected.

In this work, we report a systematic XAS study on the strained Nd_{1-x}Ca_xMnO₃ (NCMO- x) thin films with $x=0$ to 0.8. The reason for choosing the system of NCMO- x is that the tolerance factor, defined as $t=(r_{Nd/Ca}+r_O)/\sqrt{2}(r_{Mn}+r_O)$, is between 0.900 and 0.915, which is smaller than that in (La,Sr)MnO₃ ($t\sim 0.930$), thus generating a relatively stronger lattice distortion.²⁵ In addition, the Ca-doping could raise the population of e_g unoccupied state to enhance the intensity of the corresponding XAS spectra. The goal of this work is to provide an experimental evidence on the strain/doping effects on the JT splitting in the CMR films.

The NCMO- x thin films with $x=0$ to 0.8 are deposited on LaAlO₃ (LAO) single-crystal substrate by using the pulsed laser deposition with a KrF (248 nm) laser in the flowing O₂ atmosphere of 50 mTorr at the temperature of 800 °C. Sintered targets of stoichiometric single-phase oxides of Nd₂O₃, CaCO₃, and MnO₂ are used for ablation at an energy density of ~ 2 J/cm². The thickness of film is controlled by the deposition time and around 100 nm for all samples. The phase purity of all the films is analyzed with x-ray diffraction (XRD) using Bruker D8 system. The XAS experiments on NCMO- x thin films are performed at the beamline 05B2-EPU at the National Synchrotron Radiation Research Center of Taiwan using the end station photoemission electron microscopy.

X-ray diffraction patterns exhibit only (00 l) lines for both the NCMO- x thin films and the LAO substrate as shown in Fig. 1(a), indicating good crystalline structures of these films with a preferential growth along the c -axis. The c lattice parameters of all thin films are determined from the (002) d -spacing and plotted against x as open symbols in Fig. 1(b), with the dashed line marking the c -parameter of LAO and the solid symbols representing the data of bulk NCMO- x .²⁶ Since the b -parameter of the bulk sample with $x<0.3$ is much larger than that of LAO substrate and it decreases with increasing x , the compressive strain for $x=0$ and 0.1 is relatively greater than the highly doped ones. Therefore, the c -parameter of NCMO- x film first keeps as a

^{a)}Author to whom correspondence should be addressed. Electronic mail: jglin@ntu.edu.tw.

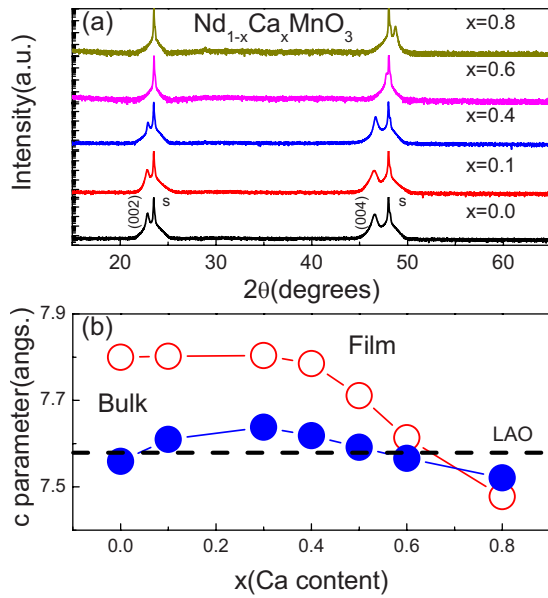


FIG. 1. (Color online) (a) The XRD patterns of NCMO- x films on LAO substrate with all lines being identified as (00 l). (b) The c -parameter vs Ca content for NCMO- x films and bulks with dashed line being the value for the LAO substrate.

constant value of 7.799 Å for $x < 0.4$, and starts to decrease linearly at $x=0.4$ to 7.477 Å at $x=0.8$. In addition, the variation of c -parameter with increasing x is more profound in films than the bulks, reflecting the dominant role of interface strain over the doping effect on the modulation of crystal structures. It is worthy to note that the interfacial strain changes from compressive to tensile at $x=0.8$ due to the doping-induced reduction of unit-cell of NCMO-0.8.

The changes of XAS spectra with Ca doping are analyzed on the leading features of O 1s as shown in Fig. 2 for (a) NCMO-0.1 and (b) NCMO-0.6. Following the standard analysis by using software IFEFFIT with FEFF theoretical functions,²⁷ the curve is fitted with five peaks for $x=0.1$ and six peaks for $x=0.6$, including the first structure of Mn 3d (from P1 to P4) and the second structure of Nd 5d/Ca 4d (P5 and P6). Three features of Mn 3d structure are attributed to the hybridization of O 2p with Mn t_{2g} and e_g , in which the crystal field of the MnO₆ octahedron splits the Mn 3d band into the low-energy t_{2g} and the high-energy e_g subbands. In addition to the effect of crystal field, magnetic exchange field splits each energy levels into two different polarizations of spin up \uparrow and spin-down \downarrow . The corresponding electronic structure of Mn 3d with spin polarizations and crystal-field effect is sketched in Fig. 2(c). It should be noted that $e_g\uparrow$ level could further split into $e_g\uparrow^1$ and $e_g\uparrow^2$ in the presence of JT effect. Based on this sketch, the relative energy levels of Mn 3d states can be obtained from the peak position in XAS spectra. For example, the first feature of NCMO-0.1 from 529 to 531.5 eV is assigned to a superposition of majority $e_g\uparrow^2$ and minority $t_{2g}\downarrow$ bands, which correspond to P2 at 529.6 eV and P3 at 530.7 eV, respectively. The second feature centered at 532.3 eV (P4) is attributed to the band of minority $e_g\downarrow$. On the other hand, the first pre-edge of NCMO-0.6 can be well fitted with three peaks: P1 at 528.7 eV for $e_g\uparrow^1$, P2 at 529.5 eV for $e_g\uparrow^2$, and P3 at 530.7 eV for $t_{2g}\downarrow$. It is interesting to note that P1 becomes observable in the samples of $x \geq 0.5$, implying that the absorption

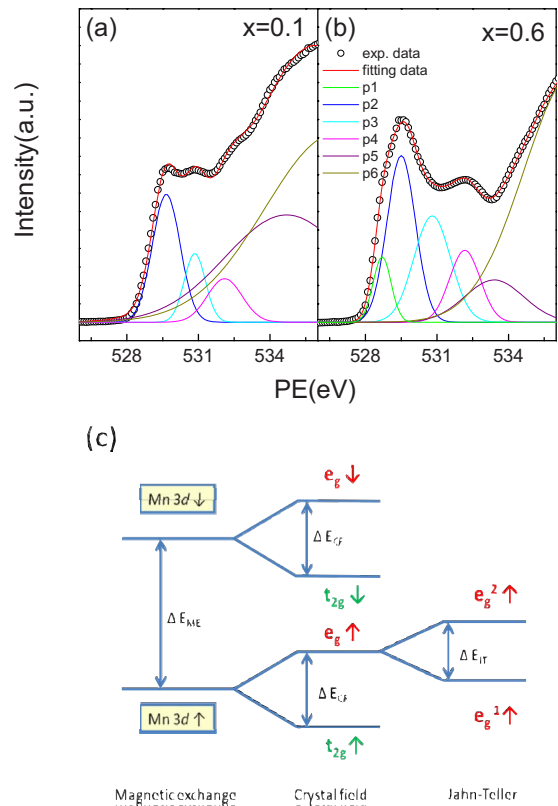


FIG. 2. (Color online) Leading feature of O 1s from 525 to 540 eV in (a) NCMO-0.1 and (b) NCMO-0.6 film; the curves are fitted with five to six peaks. (c) Schematic energy diagram of Mn 3d levels in NCMO- x films with ΔE_{ME} , ΔE_{CF} , and ΔE_{JT} denoted as the magnetic exchange interaction, crystal field splitting, and JT distortion, respectively.

of $e_g\uparrow^1$ gradually enhances with x and becomes strong enough only for $x \geq 0.5$.

In Fig. 3(a) the position of peak i (PE $_i$ with $i=1-4$) versus the Ca content (x) is plotted, indicating that the PE-value of P3 and P4 slightly increases with increasing x , while

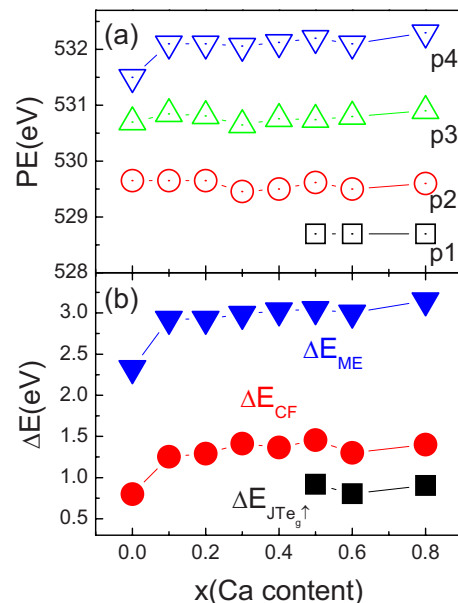


FIG. 3. (Color online) (a) Plot of all positions of peaks in the first structure with various Ca content. P1, P2, P3, and P4 represent the $e_g\uparrow^1$, $e_g\uparrow^2$, $t_{2g}\downarrow$, and $e_g\downarrow$ bands, respectively. (b) Plot of energy parameters ΔE_{ME} , ΔE_{CF} , and ΔE_{JT} in the first structure of O 1s spectra for various Ca content.

that of P2 is near a constant with increasing x . It suggests that the combined effects of strain and doping may cause a gentle modulation in the energy level for $e_g \uparrow^2$ and $e_g \downarrow / t_{2g} \downarrow$. Based on the differences between various energy levels, several important parameters can be derived, including the magnetic exchange energy $\Delta E_{ME} = PE4 - (PE2 + PE1)/2$, the crystal field energy $\Delta E_{CF} = PE4 - PE3$ and the JT distortion energy $\Delta E_{JT} = PE2 - PE1$. The results of various energy parameters versus Ca-content are plotted in Fig. 3(b). With increasing the content of Ca from zero to 0.1, ΔE_{ME} first jumps from 2.32 to 2.92 eV with x from 0 to 0.1 and then near linearly increases to 3.02 eV at $x=0.8$. Meanwhile, ΔE_{CF} increases greatly from 0.76 to 1.20 eV for x changing from 0 to 0.1 and then keeps as 1.45 ± 0.05 eV for $x \geq 0.1$. Most interestingly, the value of ΔE_{JT} is estimated as $\sim 0.8 \pm 0.1$ eV for the samples with $x \geq 0.5$, which is about half of the value predicted for LaMnO_3 .¹⁴ The appearance of P1 for $x \geq 0.5$ [as seen in Fig. 3(a)] and the small value of ΔE_{JT} suggests that JT splitting can be detected with XAS only when the $e_g \uparrow^1$ band has significant amount of unoccupied states.

In conclusion, the electronic structures of strained $\text{Nd}_{1-x}\text{Ca}_x\text{MnO}_3$ films with $x=0-0.8$ are systematically investigated via XAS. The O 1s spectrum is used to identify the energy states and is decomposed into $e_g \uparrow^1$, $e_g \uparrow^2$, $t_{2g} \downarrow$, and $e_g \downarrow$ bands. The energies of magnetic exchange, crystal field splitting and JT distortion are obtained as 2.3–3.0, 1.45, and 0.8 eV, respectively. It is worthy to mention that this XAS study demonstrates that the JT splitting of CMR system can be detected only in the sample with significant amount of holes.

This work is supported by the National Science Council of R. O. C. (Grant No. NSC-98-2811-M-002-061), and the top-project of National Taiwan University.

¹R. von Helmolt, J. Wecker, B. Hotzapfel, L. Schultz, and K. Samwer, *Phys. Rev. Lett.* **71**, 2331 (1993).

²S. Jin, T. H. Tiefel, M. McCormack, R. A. Fastnacht, R. Ramesh, and L.

H. Chen, *Science* **264**, 413 (1994).

³C. Zener, *Phys. Rev.* **82**, 403 (1951).

⁴P. W. Anderson and H. Hasegawa, *Phys. Rev.* **100**, 675 (1955).

⁵P. G. de Gennes, *Phys. Rev.* **118**, 141 (1960).

⁶K. Miyano, T. Tanaka, Y. Tomioka, and Y. Tokura, *Phys. Rev. Lett.* **78**, 4257 (1997).

⁷Y. Tomioka, A. Asamitsu, H. Kuwahara, Y. Moritomo, and Y. Tokura, *Phys. Rev. B* **53**, R1689 (1996).

⁸D. Hsu, J. G. Lin, and W. F. Wu, *Appl. Phys. Lett.* **88**, 222507 (2006).

⁹S. Mori, C. H. Chen, and S. W. Cheong, *Nature (London)* **392**, 473 (1998).

¹⁰M. Uehara, S. Mori, C. H. Chen, and S. W. Cheong, *Nature (London)* **399**, 560 (1999).

¹¹P. G. Radaelli, D. E. Cox, L. Capogna, S. W. Cheong, and M. Marezio, *Phys. Rev. B* **59**, 14440 (1999).

¹²H. Y. Huang, S. W. Cheong, P. G. Radaelli, M. Marezio, and B. Batlogg, *Phys. Rev. Lett.* **75**, 1395 (1995).

¹³S. Satpathy, Z. S. Popovic, and F. R. Vukajlovic, *Phys. Rev. Lett.* **76**, 960 (1996).

¹⁴S. Satpathy, Z. S. Popovic, and F. R. Vukajlovic, *J. Appl. Phys.* **79**, 4555 (1996).

¹⁵C. Aruta, G. Ghiringhelli, A. Tebano, N. G. Boggio, N. B. Brookes, P. G. Medaglia, and G. Balestrino, *Phys. Rev. B* **73**, 235121 (2006).

¹⁶C. T. Chen, *Nucl. Instrum. Methods Phys. Res. A* **256**, 595 (1987).

¹⁷F. M. F. de Groot, M. Griioni, J. C. Fuggle, J. Ghijsen, G. A. Sawatzky, and H. Petersen, *Phys. Rev. B* **40**, 5715 (1989).

¹⁸F. M. F. de Groot, J. C. Fuggle, B. T. Thole, and G. A. Sawatzky, *Phys. Rev. B* **41**, 928 (1990).

¹⁹M. Croft, D. Sills, M. Greenblatt, C. Lee, S. W. Cheong, K. V. Ramanujachary, and D. Tran, *Phys. Rev. B* **55**, 8726 (1997).

²⁰T. Saitoh, A. E. Bocquet, T. Mizokawa, H. Namatame, A. Fujimori, M. Abbate, Y. Takeda, and M. Takano, *Phys. Rev. B* **51**, 13942 (1995).

²¹H. L. Ju, H. C. Sohn, and K. M. Krishnan, *Phys. Rev. Lett.* **79**, 3230 (1997).

²²Y. Murakami, D. Shindo, H. Chiba, M. Kikuchi, and Y. Syono, *Phys. Rev. B* **59**, 6395 (1999).

²³T. Yanagida, Y. Saitoh, Y. Takeda, A. Fujimori, H. Tanaka, and T. Kawai, *Phys. Rev. B* **79**, 132405 (2009).

²⁴D. Y. Cho, S. J. Oh, D. G. Kim, A. Tanaka, and J. H. Park, *Phys. Rev. B* **79**, 035116 (2009).

²⁵E. Dagotto, *Nanoscale Phase Separation and Colossal Magnetoresistance* (Springer, New York, 2002).

²⁶K. Liu, X. W. Wu, K. H. Ahn, T. Sulchek, C. L. Chien, and J. Q. Xiao, *Phys. Rev. B* **54**, 3007 (1996).

²⁷B. Ravel and M. Newville, *J. Synchrotron Radiat.* **12**, 537 (2005).